Received: 7 January 2021 | Revised: 27 September 2021 | Accepted: 6 November 2021

DOI: 10.1002/stc.2891

RESEARCH ARTICLE

WILEY

Instantaneous identification of densely instrumented structures using line topology sensor networks

Said Quqa | **Luca Landi** | **Pier Paolo Diotallevi**

Department DICAM, University of Bologna, Bologna, Italy

Correspondence
Said Quqa, Department DICAM, University of Bologna, Viale Risorgimento 2, Bologna 40136, Italy.
Email: said.quqa2@unibo.it

Summary

In this paper, a new strategy for vibration-based structural health monitoring is proposed, specifically designed for smart sensors with edge computing capabilities organized in a line topology. This solution is aimed at maximizing resource optimization and enables the identification of modal parameters even for large or densely instrumented structures, where star-topology monitoring systems are typically unsuitable. In particular, an efficient data management procedure is proposed to reduce data transmission, thus improving efficiency and minimizing maintenance interventions for battery replacement in wireless applications. The maximum volume of transmitted data can be selected by the user, based on the specific requirements of the network. Although the considerable reduction of data size, the proposed approach enables accurate estimation of the structural parameters in challenging scenarios where other techniques generally fail. Modal parameters are identified in an online fashion, enabling near real-time detection and localization of early damage. Applications to a real case study instrumented with a dense sensor network show the effectiveness of the proposed approach and the possibility of localizing structural defects in slightly damaged civil structures.

KEYWORDS

damage identification, large structure, modal identification, nonstationary signal, time-frequency analysis, wireless sensor network

1 | INTRODUCTION

Vibration-based structural health monitoring (SHM) techniques have been largely used in the last decades to evaluate the state of health of monumental buildings, civil structures, infrastructures, and aerospace components.[1–5] Real-time analyses and on-site decision making may be essential for some of these applications. Scour can rapidly compromise stiffness of bridge foundations, often resulting in excessive movements or even collapse,[6] tuned mass dampers may require retuning,[7] and prompt fault detection is of the utmost importance to ensure the safety of aircraft. Moreover, time-varying systems are completely identified only if time information is considered in the description of the structural behavior.[8,9] However, the batch offline implementation of most traditional modal identification algorithms does not enable real-time applications. Identification methods involving signal windowing have thus been proposed, showing

however several limitations due to computational complexity, which is mainly related to redundancy in computation. Time-frequency representations (TFRs) obtained through the short-time Fourier transform (STFT) are usually generated considering an appropriate overlap in signal windowing to avoid loss of information.[10] The wavelet transform has shown superior performance in SHM applications, becoming suitable for signal-adaptive identification algorithms.[11] Kaya and Safak[12] used running time windows to keep track of variations in modal parameters in real time using a statistical approach, with repeated average processes. Several studies have also been conducted for extending blind source separation (BSS) techniques in real-time implementation, especially for applications in the electrical engineering field. A significant deal of research is indeed related to equivariant adaptive separation via independence (EASI) algorithms, which are generally affected by complexity issues. Amini and Ghasemi[13] attempted to address this problem presenting an EASI method for SHM applications in which the unmixing matrix used during decomposition is recursively updated. Moreover, efficient algorithms based upon recursive updates of the monitored parameters through low-rank perturbations have shown good performance and applicability for fault detection.[14] Bhowmik et al.[7] presented an approach based on recursive canonical correlation analysis (RCCA) using rank-1 updates of the eigenspace at each time instant to evaluate instantaneous modal parameters in real time without recomputing eigenvectors and eigenvalues at each iteration.

All the mentioned approaches rely on centralized network schemes, as the data collected in all the instrumented locations should be analyzed at the same instant and are transmitted without performing any preprocessing operations. Their application is thus suitable for wired acquisition systems or small wireless sensor networks (WSNs) in star topology, where data can be transmitted smoothly in real time. It is instead challenging to carry out online structural identification for large or densely instrumented structures, as they generally require advanced algorithms for data routing and tree or mesh topology layouts. In particular, when WSNs are employed, these algorithms typically involve a high battery consumption due to redundant transmission.[15] Excessive battery consumption also makes frequent maintenance interventions necessary, entailing additional costs.

Recently, dense structural features have assumed particular interest.[16] Also, due to the accessible cost of the components employed in WSNs and the development of power-optimized systems[17] and advanced synchronization strategies,[18,19] dense distributions of smart nodes are increasingly used for SHM applications, as they can be exploited to study in detail the dynamic behavior of structures and accurately localize damage.[20] Jang et al.[21] developed an event-triggered system using 70 sensor nodes and two base stations. Real-time implementation has generally demonstrated unfeasible at this scale, making the use of a proprietary wireless network protocol necessary. Whelan et al.[22] developed a network with 40 nodes using a proprietary protocol that supports high-rate acquisition with minimal data loss for real-time applications.

The decentralization of data management and processing algorithms can be a valid solution to reduce transmitted data through onboard processing.[23,24] Quqa et al.[25] recently proposed a decentralized algorithm for the identification of instantaneous modal parameters based on clustered filter banks (CBFs) that enable near real-time applications using star-topology networks.

A recent branch of research is oriented towards the application of SHM algorithms to large structures and infrastructures using wireless sensing systems, facing the issues that may arise when dealing with complex network topologies.[20,21,26] In particular, line topology is particularly suitable in the case of densely distributed structures having a one-dimensional development.[27] However, in traditional applications, the weight of the data packets increases along the transmission path, becoming particularly demanding in the final portion of the network, where the nodes consume a significant amount of energy in forwarding all the data packets collected throughout the sensing system.

Decentralized sensor networks are still rarely implemented for real-time monitoring. However, distributed solutions supported by efficient algorithms for data management may have a key role when online decision making must be achieved for densely instrumented structures, such as for civil buildings and infrastructures in emergency situations.[28]

In this paper, a new algorithm for instantaneous identification of modal parameters in large or densely instrumented civil structures is proposed. This approach is usable for both wired and wireless line-topology networks, being particularly attractive for wireless solutions due to the reduced data volume involved in transmissions. The algorithm is based on the modal assurance distribution (MAD), a novel TFR that, contrary to traditional TFRs, is not dependent on the signal energy distribution in frequency. The original formulation of the MAD and a signal-adaptive algorithm for modal identification of linear time-varying structures has been recently proposed by Quqa et al.,[29] showing high performances in case of vanishing signal components and narrow-band disturbances in the input excitation, where other well-known techniques, such as the Hilbert Huang transform (HHT), generally fail. A novel data compression strategy is proposed herein to enable the near real-time updating of the MAD and the online identification of

natural frequencies and mode shapes of the structure. The power consumption and the computational effort that compete with each node of the sensing system in the proposed approach are unrelated to the network size, making the proposed scheme easily scalable.

2 | PROCEDURE OUTLINE

In this section, the theoretical background of the MAD and a related modal identification algorithm[29] is briefly reported. Then, a novel approach to reduce the weight of the collected structural response is shown, involving a factorization that can be updated using rank-1 perturbations in a computationally efficient fashion. These concepts are employed in the formulation of an original procedure for data management that enables real-time modal identification in line-topology WSNs.

2.1 | MAD and modal decomposition

The wavelet packet transform (WPT) has been widely used to decompose signals into the time-scale domain by applying high-pass and low-pass wavelet filters recursively[30] or using a bank of equivalent bandpass filters.[10] The wavelet components obtained in this way represent information of the original signal in limited frequency bands. Considering the transform level n and the sampling frequency F_s of the original signal, the width of the frequency band described by each component of the transform (2^n in total) is $f_w = F_s/2^{n+1}$.

Operating deflection shapes (ODSs) have been traditionally defined as the deflection of a structure at a particular frequency of excitation.[2] The wavelet components related to a given frequency band of each recording channel can thus be interpreted as the amplitude values of a time-dependent ODS.

The MAD is an alternative TFR for multivariate signals.[29] The idea at the base of this technique is that the instantaneous ODSs calculated at different time instants, and frequency bands considering a set of structural responses collected at multiple instrumented locations are similar to each other (i.e., their elements are proportional) only if they refer to the same modal response; indeed, due to the orthogonality property of vibration modes, the shapes related to different modes are orthogonal. Here, we assume that the ODS calculated at a resonant frequency of the structure approximates the corresponding mode shape.

In particular, let the signal x_i (e.g., the acceleration time history) recorded by a sensor deployed on the i th physical point of a linear time-varying system be

$$x_i[t] = \sum_{j=1}^{p} \phi_{i,j}^{(t)} \ddot{q}_j[t] + v_i[t] \tag{1}$$

with $x_i[t]$ denoting the t th sample of x_i, $\ddot{q}_j[t]$ is one of the first p dominant modal components of x_i, $\phi_{i,j}^{(t)}$ is the instantaneous mode shape of the j th mode, slowly varying over time, and $v_i[t]$ is a recording noise component, here assumed as white Gaussian. Considering a bandpass filter b_j with cutoff frequencies $\omega_j - \varepsilon$ and $\omega_j + \varepsilon$, where ω_k is a natural frequency of the system and ε is a sufficiently small number (compared to the difference of the natural frequencies of two consecutive structural modes), the filtered signal component can approximately be written as

$$w_{i,j}[t] \cong \phi_{i,j}^{(t)} \left(\ddot{q}_j * b_j \right)[t] + v_{i,j}[t] \tag{2}$$

where $v_{i,j}[t]$ is a filtered noise component depending on the noise floor of the sensor, which is generally negligible compared to the structural response, and $*$ is the convolution operator. Thereby, neglecting the noise component, an estimate of the j th time-varying mode shape can be obtained referring to different sensor locations and calculating the ratios between the obtained filtered components as

$$\phi_{i,j}[t] \cong \gamma_j^{(t)} \frac{w_{i,j}[t]}{w_{r,j}[t]} \tag{3}$$

where $\gamma_j^{(t)}$ is a slowly time-varying normalization factor and i,r are two different instrumented locations. The elements thus calculated for each location, keeping r as the same reference point, can be collected into the time-dependent mode shape vector $\boldsymbol{\phi}_j[t]$. It should also be noted that employing bandpass filters with cutoff frequencies slightly different from those used above, say ω_j and $\omega_j + 2\varepsilon$, Equation 3 can still be considered as an accurate estimate of the shape of the j th mode. The frequency range where this assumption can be considered admissible depends on the dynamic features of the structure and on the specifics of the sensing devices. In particular, damping generally increases the frequency band of a given modal response, making this range wider. On the other hand, the noise floor of the sensing devices lets $v_i[t]$ prevail over modal responses when distancing from ω_j values, and thus, it reduces the accuracy of mode shapes evaluated far from the resonant frequency.

Therefore, the instantaneous ODS $\varphi_{i,k}[t]$ calculated using Equation 3 for the generic kth frequency band, that is, using a narrow bandpass filter with a central frequency equal to ω_k, will be similar to $\varphi_{i,k+1}[t]$ if the k th band is close to a resonant frequency of the system. On the other hand, if the noise component prevails in the considered frequency bands, the related ODSs will be formed of filtered noise components, randomly varying for different neighboring k values.

The MAD is a map in the time-frequency plane that indicates the "similarity" of neighboring ODSs obtained by processing the channels of a multivariate signal through a bank of narrow-band filters. In particular, the WPT is used as a filtering operator which decomposes each channel into different wavelet components, each associated with a different frequency band. In the classical WPT algorithm, the wavelet components are downsampled by a factor 2^n after being calculated using the equivalent wavelet filter bank. The output is indeed critically sampled.

Considering the vector $\boldsymbol{\varphi}_k[\xi]$ obtained using the ξth sample (after downsampling) of the wavelet components obtained using the filter b_k, here assumed as the equivalent filter associated with the k th output component of the WPT, the MAD is a matrix containing the following values:

$$m_k[\xi] = \frac{\left|\boldsymbol{\varphi}_k^T[\xi]\boldsymbol{\varphi}_{k+1}[\xi]\right|^2}{\left(\boldsymbol{\varphi}_k^T[\xi]\boldsymbol{\varphi}_k[\xi]\right)\left(\boldsymbol{\varphi}_{k+1}^T[\xi]\boldsymbol{\varphi}_{k+1}[\xi]\right)} \tag{4}$$

where the time dependency is given by ξ, that is, the column index of the MAD, while the frequency is discretized into narrow bands represented by the k index, which indicates the row index of the distribution. The values of the MAD are thus numbers in the range from 0 to 1, where values close to 1 denote the presence of similar ODSs at consecutive frequency bands, while values close to 0 denote the presence of orthogonal ODSs at consecutive frequency bands. Thus, high-valued regions in the time-frequency plane indicate frequency bands close to the resonant (natural) frequencies of the system. Far from these regions, beta-distributed noise values in the range from 0 to 1 populate the time-frequency plane. The noise distribution is due to the random similarity of ODSs generated using filtered noise components of the collected signal.

Due to its physical meaning, the MAD can be employed to visualize the evolution of modal components in the time-frequency plane, not relating directly to the amplitude of the input signal in different frequency bands (i.e., on the nature of the exciting input), but rather considering instantaneous similarities in ODSs, the amplitudes of which are not taken into account in Equation 4. The robustness of this technique to narrow-band disturbances in the input excitation is shown in a previous work of the authors.[29] High-valued regions of the MAD can thus be used to extract the related ODSs, which are likely to represent an estimate of the mode shapes of the system. A recently proposed modal identification method[29] is based on this concept and consists of reconstructing the decoupled modal responses by applying the inverse wavelet packet transform (IWPT) to the wavelet components that generate MAD values lying over a user-defined threshold. Upon reconstructing the modal responses $x_{i,j}[t]$, these can be employed to obtain an estimate of the time varying mode shapes of the system as

$$\phi_{i,j}[t] = \frac{x_{i,j}[t]}{x_{r,j}[t]} \tag{5}$$

while instantaneous natural frequencies can be simply calculated by applying the Hilbert transform to $x_{i,j}[t]$.

The decomposition of the structural response into decoupled modal contributions involves the processing of all the structural responses collected at different locations simultaneously, making the procedure unsuitable for decentralized

systems. Besides, the use of MAD-based identification procedures employing WSNs may be demanding in terms of data transmission, making the application to large structures particularly challenging.

2.2 | Factorization of the collected data

The instantaneous ODS vectors used in Equation 4 can be expressed as

$$\boldsymbol{\varphi}_k = \boldsymbol{\psi}_k^T \mathbf{X} \tag{6}$$

where $\boldsymbol{\psi}_k$ is the impulse response of the equivalent wavelet filter associated with the k th frequency band and $\mathbf{X}$ is the input matrix, that is, a matrix formed of column vectors containing the structural responses collected by different acquisition channels. In this section, the time dependence of $\mathbf{X}$ and $\boldsymbol{\varphi}_k$ will not be specified for simplicity. However, $\boldsymbol{\varphi}_k$ is the ODS evaluated at the ξth time instant, using the input matrix $\mathbf{X} = [\mathbf{x}_1[t-\tau+1,t],...,\mathbf{x}_r[t-\tau+1,t]]^T \in \mathbb{R}^{\tau \times r}$, where $\mathbf{x}_i[t_1,t_2]$ is a vector containing the samples of the collected sequence $x_i[t]$ in the time interval between t_1 and t_2, r is the number of instrumented locations, $\tau = \lambda(2^n-1)-n+1$ is the length of the equivalent wavelet filter at the transform level n, and λ is the length of the wavelet lowpass and highpass filters associated with the selected wavelet function.[25]

Substituting 6 into 4, the instantaneous MAD values can be expressed as follows.

$$m_k = \frac{\left|\boldsymbol{\psi}_k^T \mathbf{X}\mathbf{X}^T \boldsymbol{\psi}_{k+1}\right|^2}{\boldsymbol{\psi}_k^T \mathbf{X}\mathbf{X}^T \boldsymbol{\psi}_k \ \boldsymbol{\psi}_{k+1}^T \mathbf{X}\mathbf{X}^T \boldsymbol{\psi}_{k+1}} \tag{7}$$

Moreover, considering the singular value decomposition (SVD) of the input matrix $\mathbf{X} = \mathbf{U}\boldsymbol{\Sigma}\mathbf{V}^T$, an approximation of $\mathbf{X}$ can be expressed as a function of its most relevant singular vectors (and values) considering a truncated SVD

$$\mathbf{X} \approx \widehat{\mathbf{U}}\widehat{\boldsymbol{\Sigma}}\widehat{\mathbf{V}}^T \tag{8}$$

where the columns of matrices $\widehat{\mathbf{U}}$ and $\widehat{\mathbf{V}}$ contain the first s left and right singular vectors of $\mathbf{X}$, respectively, while $\widehat{\boldsymbol{\Sigma}}$ is a diagonal matrix containing the first s singular values (SVs). In order to have a good approximation of $\mathbf{X}$ in Equation 8, the s parameter can be selected according to the criterion proposed by Gavish and Donoho,[31] which allows determining the optimal rank of $\widehat{\mathbf{U}}$ and $\widehat{\mathbf{V}}$ to reconstruct signals containing either a known or unknown noise level. In the mentioned approach, the threshold to select the most relevant SVs is calculated as a function of the aspect ratio (r/τ) of the input matrix and the median of its SVs.

In the numerator of Equation 7, the correlation matrix of the input can thus be expressed as $\mathbf{X}\mathbf{X}^T \approx \widehat{\mathbf{U}}\boldsymbol{\Sigma}^2\widehat{\mathbf{U}}^T$. Also, assuming $\boldsymbol{\gamma}_k^T = \boldsymbol{\psi}_k^T\widehat{\mathbf{U}}$, an estimate of the instantaneous MAD values is given by the following.

$$m_k \approx \frac{\left|\boldsymbol{\gamma}_k^T \boldsymbol{\Sigma}^2 \boldsymbol{\gamma}_{k+1}\right|^2}{\boldsymbol{\gamma}_k^T \boldsymbol{\Sigma}^2 \boldsymbol{\gamma}_k \ \boldsymbol{\gamma}_{k+1}^T \boldsymbol{\Sigma}^2 \boldsymbol{\gamma}_{k+1}} \tag{9}$$

2.3 | Low-rank updates of the factorization

As it will be discussed later, in some applications, it may be convenient to build the input matrix by progressively increasing the number of columns of $\mathbf{X}$, that is, appending single columns to the input matrix, leaving the remaining part unchanged. In this case, the SVD of $\mathbf{X}$ can be first calculated using only a subset of its columns (i.e., only a subset of recording channels) and then updated through rank-1 perturbations, as shown by Brand,[32] to include the information contained in the remaining columns.

Let $\mathbf{U\Sigma V}^T$ be the SVD of $\mathbf{X}_c$, which is the matrix formed of the first c columns of $\mathbf{X}$. The decomposition of $\mathbf{X}_{c+1}$ can be written in the form $\mathbf{U\Sigma}\left[\mathbf{V}^T\ \mathbf{0}\right]+\mathbf{ab}^T$, where $\mathbf{a}\in\mathbb{R}^\tau$ contains the elements of $x_{c+1}[t-\tau+1,t]$, $\mathbf{b}=[0,0,...,1]^T\in\mathbb{R}^{c+1}$, and $\mathbf{0}$ is a zero-valued column vector. The updated matrices of the decomposition $\widetilde{\mathbf{U}}\widetilde{\mathbf{\Sigma}}\widetilde{\mathbf{V}}^T=\mathbf{U\Sigma}\left[\mathbf{V}^T\ \mathbf{0}\right]+\mathbf{ab}^T$ can be calculated through the following steps[32]:

1. Calculate the vector

$$\boldsymbol{\alpha}=\mathbf{a}-\mathbf{UU}^T\mathbf{a} \tag{10}$$

and its norm $\|\boldsymbol{\alpha}\|$;

2. Compute the SVD of the matrix

$$\mathbf{K}=\begin{bmatrix}\mathbf{\Sigma} & \mathbf{U}^T\mathbf{a}\\ \mathbf{0} & \|\boldsymbol{\alpha}\|\end{bmatrix} \tag{11}$$

obtaining $\mathbf{K}=\mathbf{YHZ}^T$;

3. Update the SVD matrices as

$$\widetilde{\mathbf{U}}\leftarrow[\mathbf{U}\ \overline{\boldsymbol{\alpha}}]\,\widehat{\mathbf{Y}} \tag{12}$$

$$\widetilde{\mathbf{V}}\leftarrow[\mathbf{V}_e\ \ \mathbf{b}]\,\widehat{\mathbf{Z}} \tag{13}$$

$$\widetilde{\mathbf{\Sigma}}\leftarrow\mathbf{H} \tag{14}$$

where $\overline{\boldsymbol{\alpha}}=\boldsymbol{\alpha}/\|\boldsymbol{\alpha}\|$, $\mathbf{V}_e=\left[\mathbf{V}^T\ \mathbf{0}\right]^T$, and $\widehat{\mathbf{Y}}$, $\widehat{\mathbf{Z}}$ are the truncated versions of $\mathbf{Y}$, $\mathbf{Z}$, that is, containing their first c columns.

Steps 1–3 should be repeated to include all the columns of the input matrix.

2.4 | Distributed strategy for data management

A large number of civil structures and infrastructures built in the last century are now close to, or even beyond, the end of their rated life cycle. Several types of SHM systems have been deployed to assess their integrity, initially consisting of wired solutions and more recently based on wireless sensing systems. For both these types of networks, dealing with large infrastructures is generally challenging since long cables should be deployed or high transmission ranges should be covered. In the case of WSNs, multihop transmissions have been largely employed to limit the coverage issue. In particular, due to the geometry of typical infrastructures or tall buildings, the line topology (i.e., a chain of devices formed of two-way links between one node and the next one) is particularly suitable. However, sensing nodes involved in transmitting their own collected data in addition to passing data acquired by other devices typically saturate the transmission band and rapidly drain batteries.

In this paper, a decentralized procedure is proposed for line-topology networks which involve the updating of the truncated SVD of the collected signal (i.e., the input matrix) onboard each node, before transmitting the data to the next one. Each updating involves low computational effort, being suitable for microcontrollers with a small computational footprint. Moreover, the weight of transmission packages is considerably reduced, and a user-selected upper limit can be fixed regardless of the network size. This allows the complete reconstruction of all the collected channels by a coordinator device at the end of the line-topology network without involving the transmission of all the collected samples. Besides, if the MAD is only required for visualization purposes, without the need of extracting the decoupled modal responses of the system, a more economic transmission is necessary.

A scheme of the proposed approach is reported in Figure 1. In particular, all the nodes of the network, synchronized to the same time reference, form an array of the sampled signal, for example, the acceleration response of a physical point of the structure, of length τ. The first node of the network initializes the data management procedure by transmitting the collected array to the second node. Up to the s th node, each device appends the collected array to the received matrix and proceed with the transmission. In this phase, the weight of transmitted packets grows linearly with the number of nodes. Onboard the s th node, upon appending the collected array, an SVD of the matrix of collected signals $\mathbf{X}_s$ is performed to obtain the matrices $\mathbf{U}$, $\mathbf{V}$, and $\mathbf{\Sigma}$, such that $\mathbf{X}_s = \mathbf{U}\mathbf{\Sigma}\mathbf{V}^T$. This process is performed in the "economy" mode, which removes zero rows in the $\mathbf{\Sigma}$ matrix. The decomposition matrices are then transmitted to the next node. This step involves the transmission of $s(\tau+s+1)$ elements since $\mathbf{\Sigma}$ is a diagonal matrix.

From the s th to the r th node, which is the last sensing node of the network, the array of the collected signal is used as an updating $\mathbf{a}$ vector, as shown in Section 2.3. In particular, $\widetilde{\mathbf{U}}$, $\widetilde{\mathbf{V}}$, and $\widetilde{\mathbf{\Sigma}}$ are obtained by updating the received decomposition matrices and truncated to a rank equal to s, generating matrices $\widehat{\mathbf{U}}$, $\widehat{\mathbf{V}}$, and $\widehat{\mathbf{\Sigma}}$. The obtained matrices are thus transmitted to the next node. In this phase, the number of elements transmitted from a node i to the next one is $s(\tau+i+1)$. It is worthy to note that, in the case of a traditional append-and-transmit procedure in a line-topology network, the weight of transmitted packets would be τi, with $i=1,...,r$. For large networks, s is generally much lower than r, and the convenience of using the procedure proposed is evident. Indeed, the power consumption of wireless sensing systems typically entails the most demanding part of node operations, especially for long-distance transmission.[33] The maximum weight of transmitted packets can be fixed by selecting a suitable s parameter. This selection can be made by following the criterion proposed by Gavish and Donoho,[31] applied to a complete input matrix collected before implementing the decentralized procedure. Moreover, the computational complexity to perform the update onboard each node is in the order of $O(\tau s+s^3)$.[32]

At the end of the network, a coordinator device is generally installed to gather the transmitted datasets and make it available to the user. It usually has a microcontroller or microprocessor with a larger computational footprint with respect to the other sensing nodes since filtering or other signal processing operations may be performed at this point to reduce the data weight before cloud uploading or local storing. Here, an estimate of the complete set of collected signals can be reconstructed as shown in Equation 8. This set forms a multivariate signal which can be employed to obtain the decoupled modal responses through the method proposed in Section 2.1.

It should be noted that, according to Equation 9, if only the MAD should be calculated in the monitoring process, the $\mathbf{V}$ matrix is not necessary and can thus not be updated and transmitted, reducing both the computational effort and the packet weights; indeed, in this case, the transmitted element would be $s(\tau+1)$ for nodes $i>s$.

2.5 | Real-time modal identification

At the end of the data collection process, an approximation of the acquired signal in the interval $[t-\tau+1,\ t]$ can be reconstructed using Equation 8. A set of instantaneous deflection shapes referred to the ξth instant can then be calculated through Equation 6, and the MAD at the same instant can be obtained using Equation 4 or 9. At this point, the

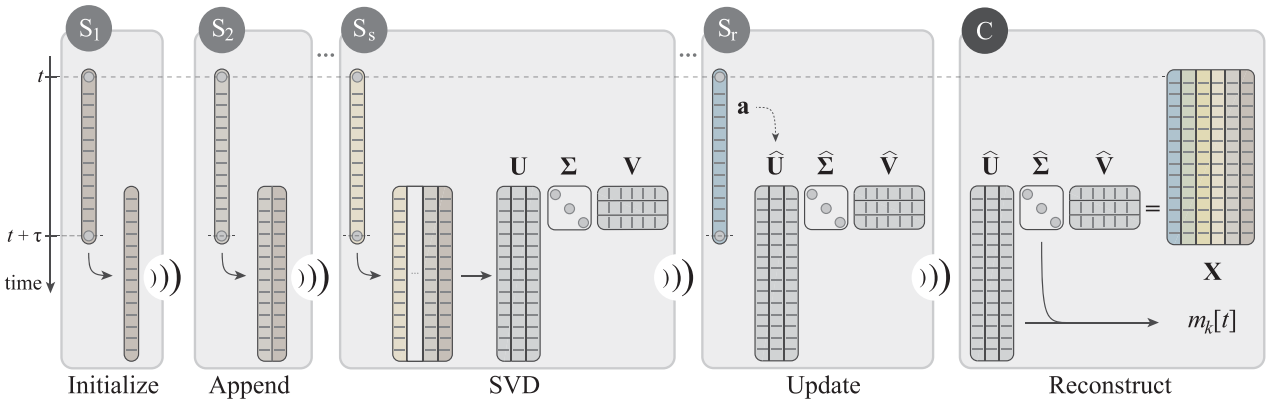

FIGURE 1 Outline of the proposed procedure for data acquisition

proposed identification procedure involves the selection of ODSs that generate high MAD values using a threshold θ, as shown in Figure 2. In order to identify the instantaneous mode shapes of the system, the set of selected ODSs are partitioned into p clusters using the k-means algorithm. The average curve obtained for each cluster is then assumed as an identified mode shape.

It is worthy to note that the traditional k-means algorithm is unable to discard outliers from noisy distributions. The thresholding operation performed using the MAD is thus necessary to obtain robust identification outcomes. Moreover, the application of the k-means algorithm needs the number of clusters as a setup parameter. However, in modal identification problems, this parameter (here denoting the number of identified modes) is not known a priori. Several methods have been proposed in the literature to identify the optimal number of clusters. In this study, the silhouette-based approach is used,[34] where silhouette values (i.e., a measure of how similar an object is to its own cluster compared to other clusters, ranging from -1 to 1) are calculated for different setups, that is, different values of p. The setup where a maximum silhouette value is reached is selected as the optimal setup. This procedure requires to apply the k-means algorithm multiple times. However, upon the selection of the optimal p parameter, this value can be employed for the long-term identification procedure, as it will be shown in the Section 3.

In real-time applications, variants of the k-means algorithm or other clustering algorithms able to handle streaming data should be employed. In this work, an online variant of the k-means algorithm is used, consisting of the following steps:

1. Apply the traditional k-means algorithm to the set of $\boldsymbol{\varphi}_k[\xi]$ with $k=1,...,2^n$ and evaluate the p centroids having coordinates described by vectors $\boldsymbol{\mu}_j[\xi]$.
2. At time instant $\xi+1$, calculate the distance between each vector $\boldsymbol{\varphi}_k[\xi+1]$ and each centroid coordinate vector $\boldsymbol{\mu}_j[\xi]$, and assign each vector $\boldsymbol{\varphi}_k[\xi+1]$ to the cluster with the closer centroid.
3. Update the centroid coordinates as

$$\boldsymbol{\mu}_j[\xi+1]=\alpha\boldsymbol{\mu}_j[\xi]+(1-\alpha)\,\overline{\boldsymbol{\varphi}}_j[\xi+1] \tag{15}$$

where $\overline{\boldsymbol{\varphi}}_j[\xi+1]=\frac{1}{l}\sum_{k=1}^{n_j}\boldsymbol{\varphi}_k[\xi+1]$ is the mean of the $\boldsymbol{\varphi}_k[\xi+1]$ vectors assigned to the j th cluster, while α is a user-defined "forgetting factor."

Following the application of the k-means algorithm, the wavelet components that generate the vectors $\boldsymbol{\varphi}_k$ associated with each cluster may be used to reconstruct decoupled modal responses through the IWPT. Since these responses are

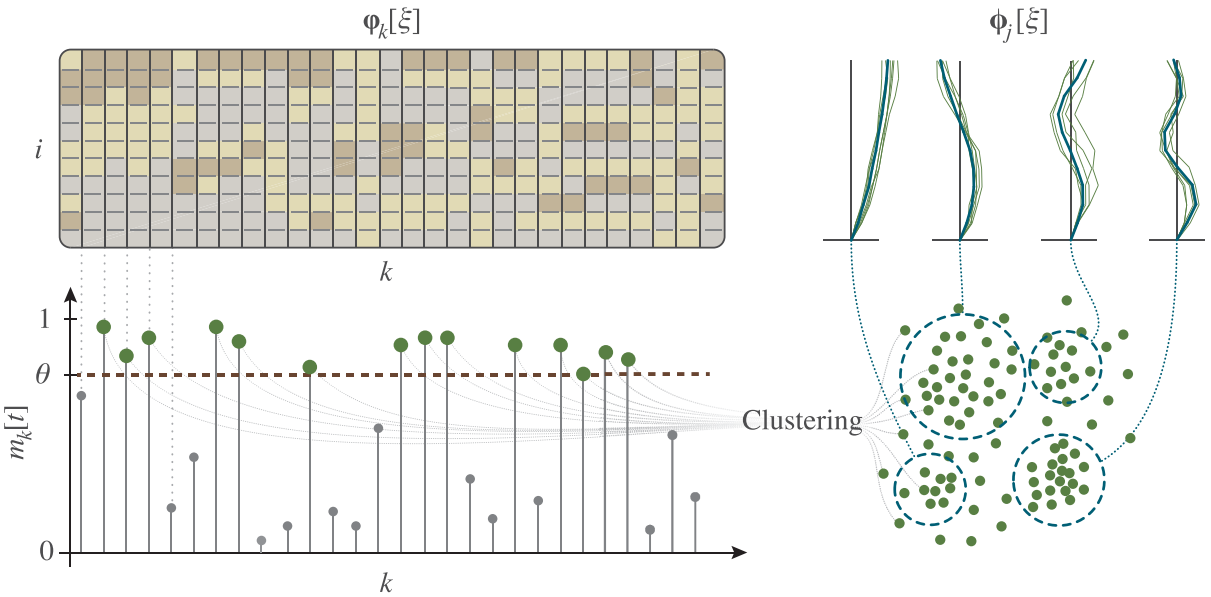

FIGURE 2 Outline of the proposed procedure for modal identification

mono-component, that is, they have a single dominant frequency, the Hilbert transform can be employed to identify the instantaneous natural frequencies of the system.

Due to noise, which can generate random similarities between consecutive ODSs (i.e., $\boldsymbol{\varphi}_k$ and $\boldsymbol{\varphi}_{k+1}$), spurious elements can be included in the clustering procedure, affecting the accuracy of the identified instantaneous modal parameters. The robustness of the method may be improved by calculating averaged modal parameters using different ξ instants or applying filtering techniques to the identification outcomes. The method proposed herein can be applied to identify modal parameters either in a continuous fashion or in periodic inspection intervals.

3 | APPLICATIONS

The procedure proposed in this paper for data management and modal identification is herein applied to a real densely instrumented case study. The benchmark shown in this paper is also analyzed in a previous work of the authors,[29] where a centralized identification algorithm, namely, the decomposition algorithm based on modal assurance (DAMA), is employed for modal identification using 4 sensing nodes. Conversely, in this paper, the data are processed simulating the use of a line-topology smart WSN consisting of 15 sensors, where the signal collected at different instrumented locations is used to update the identification results through rank-1 perturbations onboard the sensing nodes, employing the framework of the algorithm presented in the previous sections.

This section aims to show that the denser distribution of sensor leads to more accurate identification results. Besides, no relevant information is lost by applying the presented strategy for data compression, while the volume of the transmitted data can be considerably reduced compared to a traditional implementation. The suitability of the procedure for early damage localization is shown by studying the structural conditions related to different low-damage scenarios.

3.1 | Description of the case study

The case study analyzed in this paper is a slice of a full-scale 7-story reinforced concrete building, schematized in Figure 3.[35] The lateral force resisting system consists of two perpendicular 20-m-high cantilever walls. Horizontal slabs delimitate each level of the structure. Torsional stability is provided by a post-tensioned column, and the vertical loads are directed to the foundation through 4 gravity columns supporting the floor slabs. The structure was tested on a shaking table at the University of California, San Diego, within the George E. Brown Jr. Network for Earthquake Engineering Simulation program. The experimental campaign consisted of both seismic, ambient, and white noise base excitation tests. In particular, the second was obtained by locking the shaking table, while the third consisted of a banded white noise (in the range 0.25–25 Hz) process with a root mean square (RMS) amplitude of 0.03 g.[36]

The seismic tests were designed to induce progressive damage to the structure. Several historical earthquakes of increasing intensity recorded in Southern California were employed. Moreover, before and after each seismic test, the structural response was recorded during both white noise base excitation and ambient vibration. In this paper, the structural response collected during the ambient vibration intervals before the first (here called "undamaged condition" or U) and after the first two seismic tests (D1 and D2) is used to demonstrate the efficacy of the presented method in identifying limited damage. The mentioned seismic tests were performed using the longitudinal and transverse component, respectively, of the San Fernando earthquake (1971), recorded from the Van Nuys station.

The inspection time series used in this paper (U, D1, and D2) have a duration of 458 s and a sampling frequency of 60 Hz. A unique signal, with a total duration of 1374 s, generated by appending the mentioned time series one at the end of the previous one, is employed in this study to simulate ongoing damage. Low-pass filter and downsampling of factor 4 were applied to the original signal, sampled at 240 Hz, before using the data.

The instrumentation used to collect the data consisted of MEMS-Piezoresistive sensors having an amplitude range of $\pm$5 g and voltage sensitivity of 400 mV/g. In particular, 15 channels are considered in this study, collecting longitudinal (east–west) acceleration at the base, on the web wall at each floor level, and at mid-height of each story of the structure, as shown in Figure 3. A reference for the identification results shown in the following sections of this paper is obtained using the DAMA, applied to the signal collected using a limited subset of sensors (namely, S3, S7, S11, and S15).[29]

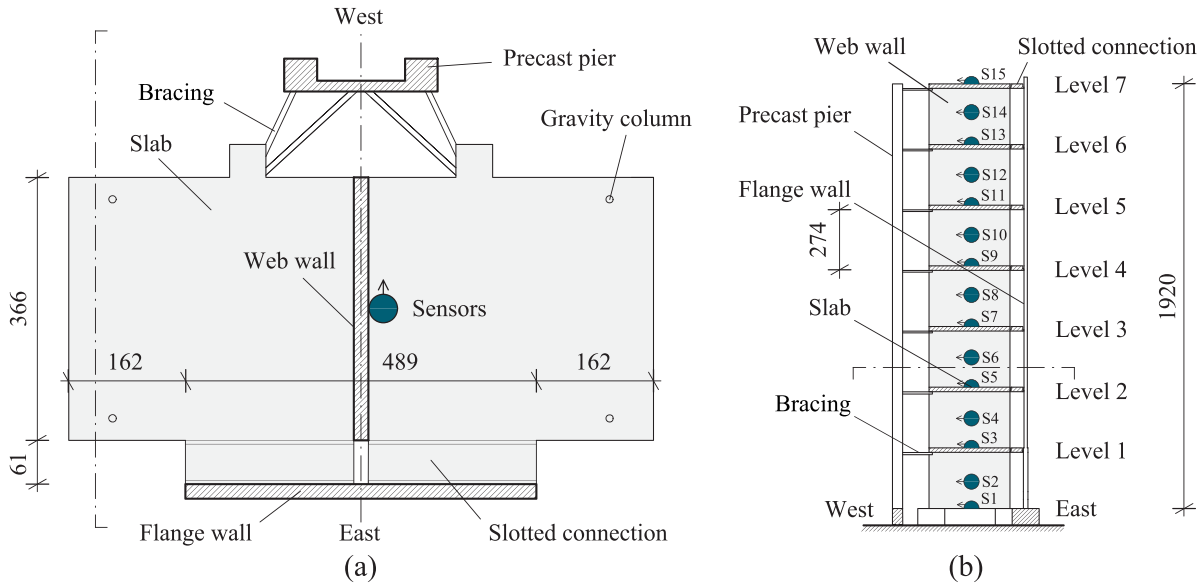

FIGURE 3 Scheme of the case study and sensor layout: (a) plan view and (b) lateral view, adapted from literature[35]

During the two seismic tests considered in this work, "slightly" and "moderate" nonlinear responses were registered. During the first test, limited yielding occurred at the base of the web wall, generating cracks up to the fourth floor and a maximum roof drift ratio (defined as the ratio between the maximum lateral displacement at the uppermost level and the distance of this level to the base of the wall) equal to 0.28%. During the second seismic test, the maximum roof drift ratio was equal to 0.75%. More details about the original testing setup and structural behavior can be found in referenced papers.[37–39]

3.2 | Discussion of the results

Before applying the modal identification algorithm, a study is conducted on the relevance of singular components (i.e., values and vectors) of the collected structural responses. In Figure 4, the 15 SVs obtained through the SVD of the original input matrix are reported on a logarithmic scale. A threshold for the selection of the most relevant components is calculated employing the method proposed by Gavish and Donoho[31] for signals with an unknown noise level. In this case, the first 5 SVs are above the selected threshold and can be used to obtain a good approximation of the input matrix.

Simulating the use of a line-topology network, in a traditional data acquisition process, the weight of the transmitted packets would increase linearly with the number of sensors. This trend is represented in Figure 5 and compared with the packet weight referred to the proposed decentralized approach. In this figure, the packet weight is expressed as the number of floating-point data values (with the single or double precision format, depending on the specific applications) that are transmitted from a node to the next one in the path to reach the end of the network. As explained in Section 2.4, the maximum packet weight can be adjusted by the user by selecting a suitable number of SVs in the approximation of the input matrix. In this study, the 5 SVs lying over the selected threshold are employed, resulting in a considerable decrement of total transmission weight. In particular, the weight of the last packet transmitted to the coordinator would be 13155 for the transmission of the original input matrix, while only 4465 for the transmission of the approximated one. Power consumption concerning transmission is approximately proportional to the packet weight; therefore, the proposed method entails a considerable power saving, especially for the last nodes. Specifically, in the considered case study, the last node undergoes a reduction of 66% in power consumption related to data transmission. This allows optimizing maintenance interventions for battery replacement since the power consumption tends to be more uniform throughout the network.

Upon selecting the number of most relevant SVs, the most suitable number of clusters for applying the proposed identification procedures is sought using the silhouette-based method. In this analysis, both the original input matrix

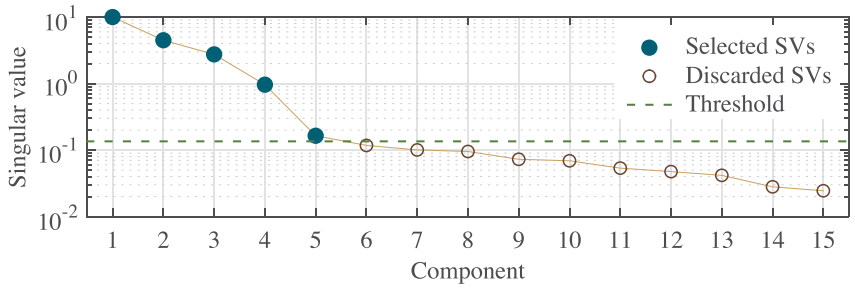

FIGURE 4 Selection of the most significant singular values

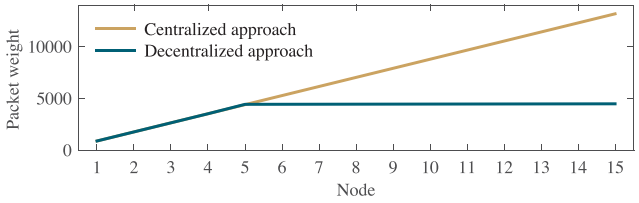

FIGURE 5 Packet weight in a line-topology network

and the approximation obtained using the first 5 singular components are used for comparison. The silhouette-based approach is applied to the ODSs obtained using the input matrices relevant to a set of different "testing" time samples. The most recurrent result over the testing samples is then assumed as the optimal p parameter. In particular, 123 testing input matrices $\mathbf{X} = [\mathbf{x}_1[t-\tau+1,t],...,\mathbf{x}_r[t-\tau+1,t]]^T$ have been selected considering different time samples t equally distributed in the complete structural response (formed of U, D1, and D2 recordings, with 41 testing samples in each of them). In Figure 6a,b, the results of this analysis are reported, referred to the case of a complete input matrix and approximated version, respectively. Each thin brown line reported in this figure is relevant to the set of ODSs computed from a given input matrix. In particular, each point of these lines indicates the average silhouette width obtained by applying the k-means algorithm with a different value of p, which is reported on the abscissa of the diagram. These lines have three different colors (from dark brown to light brown) corresponding to the test input matrices selected in different structural conditions (i.e., U, D1, and D2, respectively). For each line, the global maximum is highlighted through a circle that indicates the optimal number of clusters resulting from the analysis of the specific input matrix. The cumulative number of optimal results obtained for each p value is then calculated to improve the robustness of the selection approach. Three thick lines, referring to the cumulative number of optimal results for each p value obtained in the three structural conditions (i.e., calculated using 41 test instants each), are also reported in Figure 6. It is possible to notice that the maxima of these lines, that is, the most suitable p value for clustering, are at $p = 4$ for each structural condition and both considering the original and the approximated input matrices. This result indicates that the selection of the p parameter can generally be done in the initial phase of the procedure and then employed during the long-term identification process. Moreover, the optimal number of clusters is the same using the two versions of the input matrix, denoting that no useful information is lost during the approximation process.

The multivariate signal consisting of the 15 collected time histories in the three structural conditions is employed to obtain the MAD reported in Figure 7a. Here, high values (close to 1) are depicted in yellow, while low values (close to 0) are represented in blue. Low-valued horizontal bands can be clearly noticed in the time-component plane around the 5th and the 35th components. In this plot, the component indicated on the vertical axis represents the k index used in Equation 4. The MAD is used to select the wavelet components which generate similar ODSs (using a threshold level $\theta = 0.9$), hence discarding the components related to noise. The ODSs generated by the selected components are then partitioned using the k-means algorithms into 4 clusters, which is the optimal p parameter obtained in the previous analysis. A forgetting factor $\alpha = 0.99$ was selected to perform the online clustering procedure described in Section 2.5. A representation of the clustered components in the time-component plane is reported in Figure 7b. Here, each vector $\boldsymbol{\varphi}_k[\xi]$ is depicted in the time-component plane (indicated through the ξ and k indices, respectively) as a point having a color that depends on the assigned cluster.

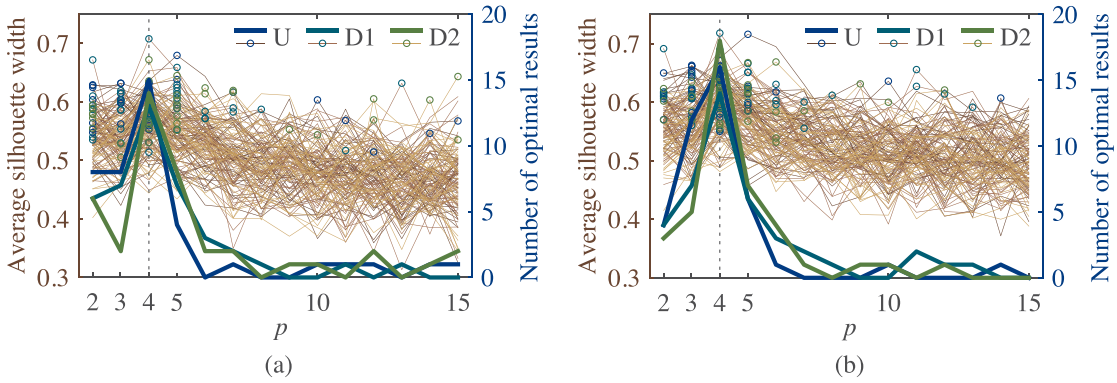

FIGURE 6 Selection of the most suitable number of clusters using (a) original input matrices and (b) approximations of the input matrices

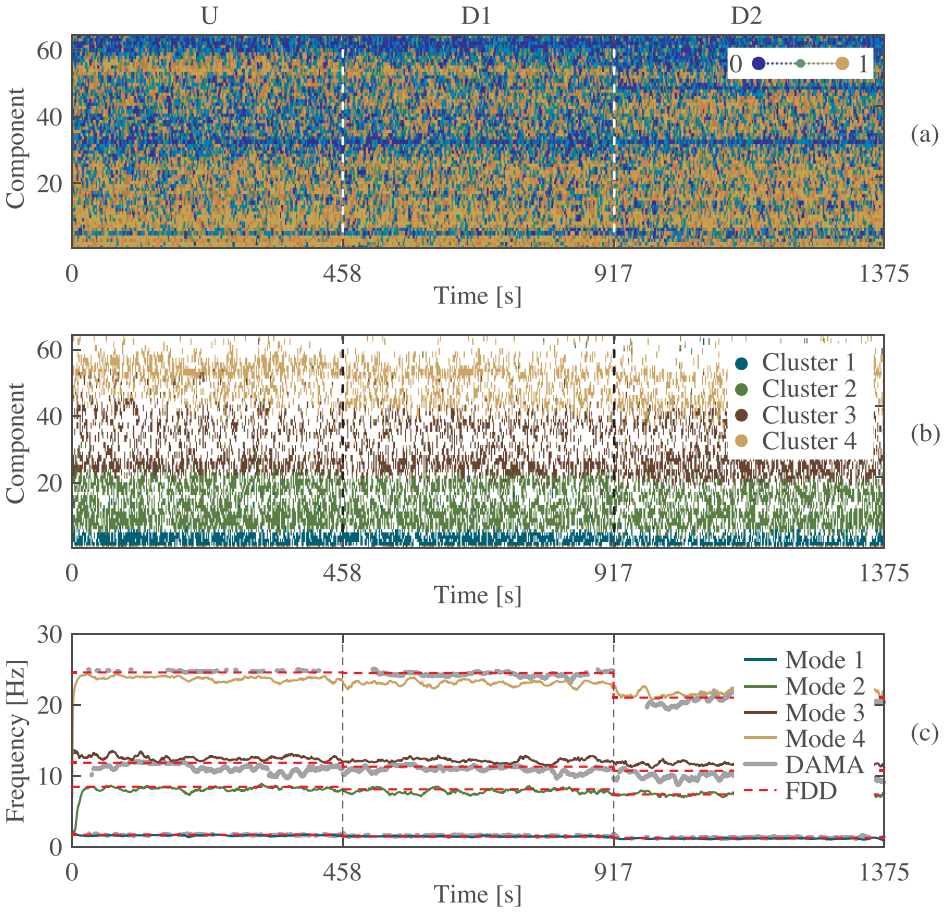

FIGURE 7 Modal assurance distribution (a), clustered components (b), and identified instantaneous frequencies (c)

The decoupled modal responses associated with each cluster are thus calculated using the IWPT, and the instantaneous frequencies are identified by applying the HT on the obtained monocomponent responses. Figure 7c shows the identified instantaneous frequencies for all the identified modes. A median filter is applied to the obtained results to improve the readability of the plot, replacing each instantaneous frequency entry with the median of 1000 neighboring entries (i.e., using a kernel of 16.67 s). In this figure, a slight decrement of the natural frequencies can be noticed when passing from condition D1 to D2, especially for modes 1 and 4.

In Figure 7c, the results obtained through the original DAMA are also reported in gray, as well as the reference values identified using the frequency domain decomposition (FDD).[40] It is possible to notice that all the results are in good agreement, especially for the first mode. However, the use of 15 sensing nodes has allowed the successful identification of 4 modes in the range 0–30 Hz, compared to the 3 modes identified using the DAMA with 4 sensors.

The reconstructed decoupled modal responses are then employed to evaluate the instantaneous mode shapes of the structure by using Equation 5. Before applying this procedure, the responses obtained at the base level (using sensor S1) are subtracted from the responses of the upper levels in order to convert the absolute horizontal acceleration measurements to relative accelerations. This step is suggested in the literature[37] to improve the results of modal identification when dealing with white noise base excitation tests. Figure 8 shows the instantaneous amplitudes of the shapes identified through the procedure proposed in this work. Slight variations can be observed when passing from condition U to D1 in modes 1 and 4, while moderate differences for all modes are noticeable when passing from D1 to D2. In particular, the shape of mode 3 in the third structural condition is considerably different from the previous conditions. This is also observable in the average shapes in right-hand side of Figure 8, where the reference shapes of the undamaged condition identified using the DAMA (employing 4 sensors) and the FDD (employing 15 sensors) are also reported. It should be noted that the second shape is not reported for the DAMA since it was not identified using the limited sensor configuration. In both the instantaneous and average representations of Figure 8, the shapes are normalized to have a unitary norm.

The identified instantaneous natural frequencies and mode shapes can be employed in SHM applications for damage identification, relying on different methods based on modal parameters. The displacement and curvature have been largely used as flexibility-based indices,[41,42] while the interpolation method has shown superior performance when the errors in the computation of the curvature may affect the results.[43] In this study, a flexibility-based approach is addressed for this purpose to provide an example of using identified parameters in SHM applications. The adopted

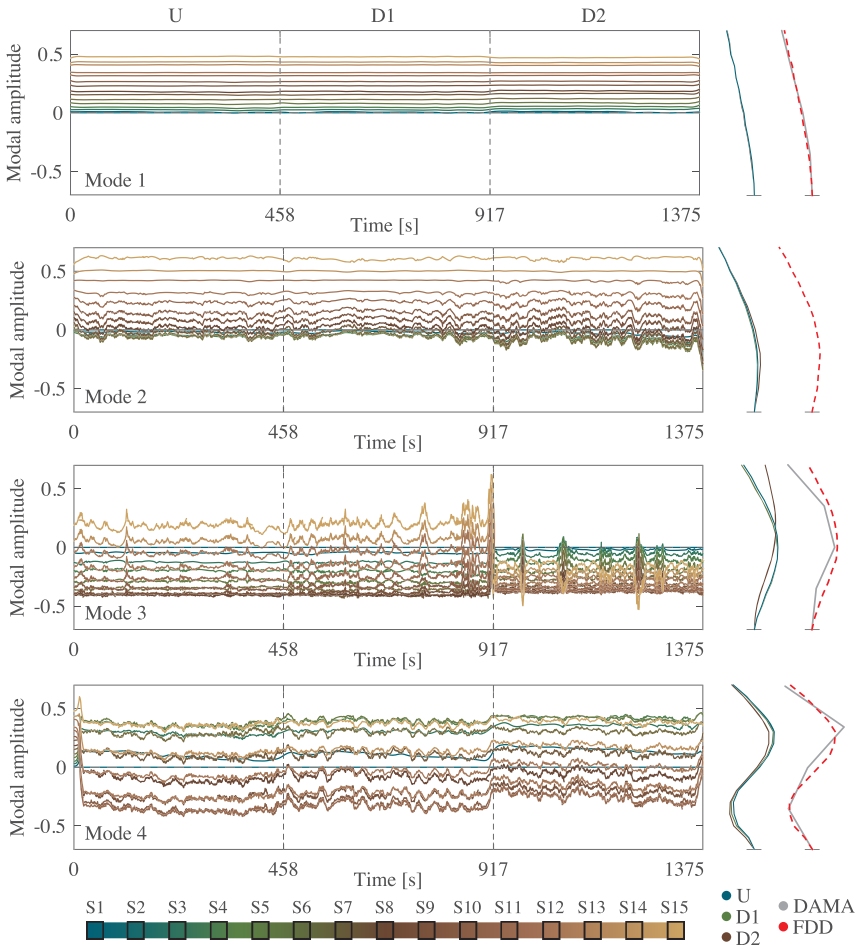

FIGURE 8 Instantaneous amplitudes of the identified modes (left) and averaged identified shapes for each condition (right)

approach consists of evaluating the uniform load surface (ULS) of the structure (which degenerates into a line— the uniform load line, ULL—for structures with one-dimensional development). In particular, the instantaneous ULL can be calculated as

$$\mathbf{u}[t] = \mathbf{F}[t]\mathbf{p} \tag{16}$$

where $\mathbf{p} = [1, ..., 1]^T \in \mathbb{R}^r$ is a unit load vector and $\mathbf{F}[t]$ is the instantaneous flexibility matrix of the system, which can be obtained as

$$\mathbf{F}[t] \approx \sum_{j=1}^{p} \frac{1}{\omega_j^2} \boldsymbol{\phi}_j[t] \boldsymbol{\phi}_j^T[t] \tag{17}$$

with ω_j denoting the j th natural circular frequency. It should be noted that $\boldsymbol{\phi}_j$ must be normalized to the masses of the system to obtain the real flexibility matrix. However, since the mass distribution over the height of the structure analyzed in this section is likely to be constant, the mass matrix is here assumed as an identity matrix. Thus, $\mathbf{F}$ is assumed as proportional to the real flexibility matrix of the structure.

In this study, the curvature of the ULL, evaluated through the central difference method, is employed as a damage-sensitive feature (DSF). Specifically, the damage index is calculated as

$$D_j[t] = \frac{\chi_{I,j}[t] - \overline{\chi}_{B,j}}{std\left(\chi_{B,j}\right)} \tag{18}$$

where $\chi_{I,j}[t]$ is the curvature at the j th node in the inspection instant, $\overline{\chi}_{B,j}$ is the mean of the curvature values at the same node in a baseline interval, and $std\left(\chi_{B,j}\right)$ is the standard deviation in the considered baseline interval. Assuming a normal distribution for the DSF, a threshold for damage localization can be selected as $\delta = 3$ in order to minimize the occurrence of false positives to less than 0.1%.[44] Therefore, if $D_j[t] > \delta$, the j th location is likely to be damaged at the t th instant. Assuming also that real damage is persistent in time, $D_j[t]$ values over the threshold for a limited time interval where the general trend is below the threshold can be considered as false positives. On the other hand, spurious $D_j[t]$ values below the threshold where the general trend exceeds it can be considered as false negatives.

Figure 9 shows the instantaneous ULL and the curvature-based damage index calculated as shown above. In particular, in Figure 9a, both the instantaneous estimates and the averaged curves representing the ULL are reported. A clear variation is noticeable when passing through different structural conditions. In Figure 9b, the values below the threshold are depicted in gray. For the condition U, some false positives are registered at the lower levels in short time intervals. On the other hand, for conditions D1 and D2, a generally positive trend is registered at the base of the structure. Moreover, the damage index grows in condition D2, and other damaged locations are identified at the mid-height of each story throughout the structure. This information corresponds to the description of the structural state, observed through the visual inspections conducted during the experimental campaign.[37–39]

4 | CONCLUSIONS

This paper presents a novel approach for the near real-time identification of modal features in civil structures instrumented with dense line-topology smart sensor networks. The method is based on the MAD that originally needs the complete dataset available to decompose the structural responses into a set of decoupled modal contributions. A new procedure for collecting data and updating the identified parameters in an online efficient manner is thus proposed, showing that no relevant information is lost due to data compression while reducing considerably the weight of transmitted data. The procedure is thus particularly promising for applications involving wireless solutions.

The method is applied to a real case study, simulating the use of a WSN. By properly selecting the number of singular components used in the factorization of the collected data matrix, the results have shown a considerable reduction in data weight, also homogenizing the power consumption throughout the network, towards the optimization of network maintenance interventions. Moreover, the approximated data matrix reconstructed at the end of the linear

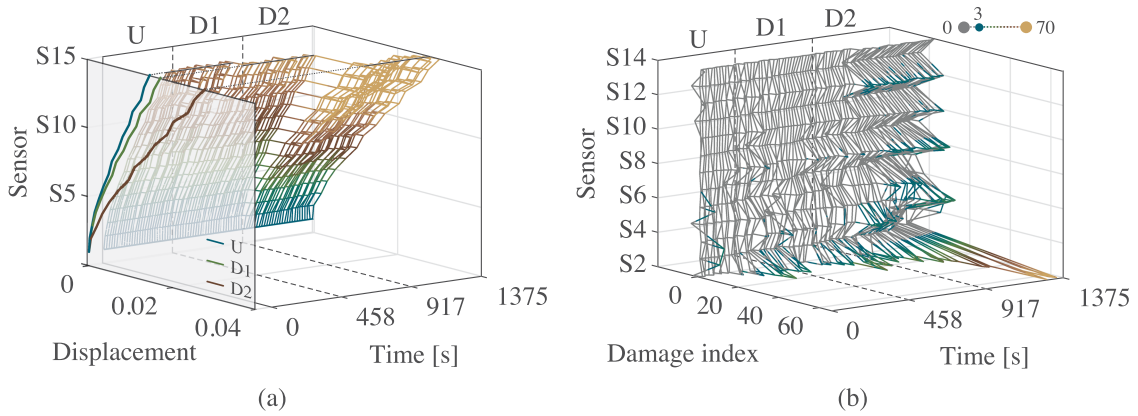

FIGURE 9 Instantaneous uniform load line (a) and damage index (b)

network (i.e., onboard a coordinator node or through cloud computing) has shown usable for identifying accurate modal parameters, which are sensitive to limited damage. In particular, a flexibility-based approach was employed to calculate the uniform load line of the structure and its curvature, which enables the prompt detection and localization of damaged structural portions.

ACKNOWLEDGMENT

The authors would like to gratefully acknowledge the availability of data recorded on the UCSD building. This research did not receive any specific grant from funding agencies in the public, commercial, or not-for-profit sectors.

CONFLICT OF INTERESTS

The authors declare that they have no known competing financial interests or personal relationships that could have appeared to influence the work reported in this paper.

DATA AVAILABILITY STATEMENT

The data that support the findings of this study are openly available in DesignSafe at https://doi.org/10.4231/D35T3G04T.

ORCID

Said Quqa https://orcid.org/0000-0001-6388-370X
Luca Landi https://orcid.org/0000-0001-7259-1186

REFERENCES

1. Fan W, Qiao P. Vibration-based damage identification methods: a review and comparative study. *Struct Health Monit*. 2011;10(1):83-111. https://doi.org/10.1177/1475921710365419
2. Brincker R, Ventura CE. *Introduction to Operational Modal Analysis*. John Wiley and Sons, Ltd; 2015. https://doi.org/10.1002/9781118535141
3. Farrar CR, Worden K. An introduction to structural health monitoring. *Philos Trans R Soc A Math Phys Eng Sci*. 1851;2007(365):303-315. https://doi.org/10.1098/rsta.2006.1928
4. Alaggio R, Aloisio A, Antonacci E, Cirella R. Two-years static and dynamic monitoring of the Santa Maria di Collemaggio basilica. *Construct Build Mater*. 2020;268:121069. https://doi.org/10.1016/j.conbuildmat.2020.121069
5. Salehi H, Das S, Chakrabartty S, Biswas S, Burgueño R. Damage identification in aircraft structures with self-powered sensing technology: a machine learning approach. *Struct Control Health Monit*. 2018;25(12):e2262. https://doi.org/10.1002/stc.2262
6. Giordano PF, Prendergast LJ, Limongelli MP. A framework for assessing the value of information for health monitoring of scoured bridges. *J Civ Struct Heal Monit*. 2020;10(3):485-496. https://doi.org/10.1007/s13349-020-00398-0
7. Bhowmik B, Tripura T, Hazra B, Pakrashi V. Real time structural modal identification using recursive canonical correlation analysis and application towards online structural damage detection. *J Sound Vib*. 2020;468:115101. https://doi.org/10.1016/j.jsv.2019.115101
8. Pakrashi V, O'Connor A, Basu B. Effect of tuned mass damper on the interaction of a quarter car model with a damaged bridge. *Struct Infrastruct Eng*. 2010;6(4):409-421. https://doi.org/10.1080/15732470701816850

9. Allen MS, Sracic MW, Chauhan S, Hansen MH. Output-only modal analysis of linear time-periodic systems with application to wind turbine simulation data. *Mech Syst Signal Process*. 2011;25(4):1174-1191. https://doi.org/10.1016/j.ymssp.2010.12.018
10. Vetterli M, Kovačević J. *Wavelets and Subband Coding*. Prentice-Hall; 1995.
11. Klepka A, Uhl T. Identification of modal parameters of non-stationary systems with the use of wavelet based adaptive filtering. *Mech Syst Signal Process*. 2014;47(1-2):21-34. https://doi.org/10.1016/j.ymssp.2013.09.001
12. Kaya Y, Safak E. Real-time analysis and interpretation of continuous data from structural health monitoring (SHM) systems. *Bull Earthq Eng*. 2015;13(3):917-934. https://doi.org/10.1007/s10518-014-9642-9
13. Amini F, Ghasemi V. Adaptive modal identification of structures with equivariant adaptive separation via independence approach. *J Sound Vib*. 2018;413:66-78. https://doi.org/10.1016/j.jsv.2017.09.033
14. Bhowmik B, Tripura T, Hazra B, Pakrashi V. First-order eigen-perturbation techniques for real-time damage detection of vibrating systems: theory and applications. *Appl Mech Rev*. 2019;71(6):1–46. https://doi.org/10.1115/1.4044287
15. Abdulkarem M, Samsudin K, Rokhani FZ, Rasid MFA. Wireless sensor network for structural health monitoring: a contemporary review of technologies, challenges, and future direction. *Struct Health Monit*. 2020;19(3):693-735. https://doi.org/10.1177/1475921719854528
16. Quqa S, Landi L, Diotallevi PP. Automatic identification of dense damage-sensitive features in civil infrastructure using sparse sensor networks. *Autom Constr*. 2021;128:103740. https://doi.org/10.1016/j.autcon.2021.103740
17. Long J, Büyüköztürk O. A power optimised and reprogrammable system for smart wireless vibration monitoring. *Struct Control Health Monit*. 2020;27(2):e2468. https://doi.org/10.1002/stc.2468
18. Fu Y, Mechitov K, Hoang T, Kim JR, Memon SA, Spencer BF. Efficient and high-precision time synchronization for wireless monitoring of civil infrastructure subjected to sudden events. *Struct Control Health Monit*. 2020;28(1):e2643. https://doi.org/10.1002/stc.2643
19. Dragos K, Theiler M, Magalhães F, Moutinho C, Smarsly K. On-board data synchronization in wireless structural health monitoring systems based on phase locking. *Struct Control Health Monit*. 2018;25(11):e2248. https://doi.org/10.1002/stc.2248
20. Pakzad SN, Fenves GL, Kim S, Culler DE. Design and implementation of scalable wireless sensor network for structural monitoring. *J Infrastruct Syst*. 2008;14(1):89-101. https://doi.org/10.1061/(ASCE)1076-0342(2008)14:1(89)
21. Jang S, Jo H, Cho S, et al. Structural health monitoring of a cable-stayed bridge using smart sensor technology: deployment and evaluation. *Smart Struct Syst*. 2010;6(5-6):439-459. https://doi.org/10.12989/sss.2010.6.5_6.439
22. Whelan MJ, Gangone MV, Janoyan KD, Jha R. Real-time wireless vibration monitoring for operational modal analysis of an integral abutment highway bridge. *Eng Struct*. 2009;31(10):2224-2235. https://doi.org/10.1016/j.engstruct.2009.03.022
23. Huang K, Yuen KV. Online dual-rate decentralized structural identification for wireless sensor networks. *Struct Control Health Monit*. 2019;26(11):e2453. https://doi.org/10.1002/stc.2453
24. Giordano PF, Quqa S, Limongelli MP. Statistical approach for vibration-based damage localization in civil infrastructures using smart sensor networks. *Inf Dent*. 2021;6(2):22. https://doi.org/10.3390/infrastructures6020022
25. Quqa S, Landi L, Diotallevi PP. Instantaneous modal identification under varying structural characteristics: a decentralized algorithm. *Mech Syst Signal Process*. 2020;142:106750. https://doi.org/10.1016/j.ymssp.2020.106750
26. Yuan S, Lai X, Zhao X, Xu X, Zhang L. Distributed structural health monitoring system based on smart wireless sensor and multi-agent technology. *Smart Mater Struct*. 2006;15(1):1-8. https://doi.org/10.1088/0964-1726/15/1/029
27. Kim S, Pakzad S, Culler D, et al. Health monitoring of civil infrastructures using wireless sensor networks. *IPSN* 2007 Proc Sixth Int Symp Inf Process Sens Networks 2007:254–263. https://doi.org/10.1145/1236360.1236395
28. Quqa S, Landi L, Diotallevi PP. Seismic structural health monitoring using the modal assurance distribution. *Earthq Eng Struct Dyn*. April 2021;eqe.3451. 50:2379–2397. https://doi.org/10.1002/eqe.3451
29. Quqa S, Landi L, Diotallevi PP. Modal assurance distribution of multivariate signals for modal identification of time-varying dynamic systems. *Mech Syst Signal Process*. 2021;148:107136. https://doi.org/10.1016/j.ymssp.2020.107136
30. Mallat SG. *A Wavelet Tour of Signal Processing*. Third ed. Academic Press; 2009. https://doi.org/10.1016/B978-0-12-374370-1.X0001-8
31. Gavish M, Donoho DL. The optimal hard threshold for singular values is $4/\sqrt{3}$. *IEEE Trans Inf Theory*. 2014;60(8):5040-5053. https://doi.org/10.1109/TIT.2014.2323359
32. Brand M. Fast low-rank modifications of the thin singular value decomposition. *Linear Algebra Appl*. 2006;415(1):20-30. https://doi.org/10.1016/j.laa.2005.07.021
33. Singh MK, Amin SI. Energy-efficient data transmission technique for wireless sensor networks based on DSC and virtual MIMO. *ETRI J*. 2020;42(3):341-350. https://doi.org/10.4218/etrij.2018-0632
34. Chiang MMT, Mirkin B. Intelligent choice of the number of clusters in k-means clustering: an experimental study with different cluster spreads. *J Classif*. 2010;27(1):3-40. https://doi.org/10.1007/s00357-010-9049-5
35. Martinelli P, Filippou FC. Simulation of the shaking table test of a seven-story shear wall building. *Earthq Eng Struct Dyn*. 2009;38(5):587-607. https://doi.org/10.1002/eqe.897
36. Conte J, Restrepo J, Panagiotou M. Shake table test of 7-story RC bearing wall building. DesignSafe-CI 2006. doi:10.4231/D35T3G04T
37. Moaveni B, He X, Conte JP, Restrepo JI, Panagiotou M. System identification study of a 7-story full-scale building slice tested on the UCSD-NEES shake table. *J Struct Eng*. 2011;137(6):705-717. https://doi.org/10.1061/(ASCE)ST.1943-541X.0000300
38. Moaveni B, He X, Conte JP, Restrepo JI. Damage identification study of a seven-story full-scale building slice tested on the UCSD-NEES shake table. *Struct Saf*. 2010;32(5):347-356. https://doi.org/10.1016/j.strusafe.2010.03.006

39. Panagiotou M, Restrepo JI, Conte JP. Shake-table test of a full-scale 7-story building slice. Phase I: Rectangular wall. *J Struct Eng*. 2011; 137(6):691-704. https://doi.org/10.1061/(ASCE)ST.1943-541X.0000332
40. Brincker R, Zhang L, Andersen P. Modal identification of output-only systems using frequency domain decomposition. *Smart Mater Struct*. 2001;10(3):441-445. https://doi.org/10.1088/0964-1726/10/3/303
41. Catbas FN, Gul M, Burkett JL. Damage assessment using flexibility and flexibility-based curvature for structural health monitoring. *Smart Mater Struct*. 2008;17(1):015024. https://doi.org/10.1088/0964-1726/17/01/015024
42. Sung SH, Jung HYJ, Jung HYJ. Damage detection for beam-like structures using the normalized curvature of a uniform load surface. *J Sound Vib*. 2013;332(6):1501-1519. https://doi.org/10.1016/j.jsv.2012.11.016
43. Giordano PF, Limongelli MP. Response-based time-invariant methods for damage localization on a concrete bridge. *Struct Concr*. 2020; 21(4):1254-1271. https://doi.org/10.1002/suco.202000013
44. Bernagozzi G, Ventura CE, Allahdadian S, Kaya Y, Landi L, Diotallevi PP. Output-only damage diagnosis for plan-symmetric buildings with asymmetric damage using modal flexibility-based deflections. *Eng Struct*. 2020;207:110015. https://doi.org/10.1016/j.engstruct.2019.110015

How to cite this article: Quqa S, Landi L, Diotallevi PP. Instantaneous identification of densely instrumented structures using line topology sensor networks. *Struct Control Health Monit*. 2022;29(3):e2891. doi:10.1002/stc.2891